Improving Motion Estimation Using Image-Driven Functions and Hybrid Scheme

Duc Dung Nguyen and Jae Wook Jeon*

Department of Electrical and Computer Engineering, Sungkyunkwan University, Korea
nddunga3@skku.edu, jwjeon@yurim.skku.ac.kr

Abstract. We introduce an alternative method to improve optical flow estimation using image data for control functions. Base on the nature of object motion, we tune the energy minimization process with an image-adaptive scheme embedded inside the energy function. We propose a hybrid scheme to improve the quality of the flow field and we use it along with the multiscale approach to deal with large motion in the sequence. The proposed hybrid scheme take advantages from multigrid solver and the pyramid model. Our proposed method yields good estimation results and it shows the potential to improve the performance of a given model. It can be applied to other advanced models. By improving quality of motion estimation, various applications in intelligent systems are available such as gesture recognition, video analysis, motion segmentation, etc.

1 Introduction

Motion estimation is still an active field in computer vision with various applications, including motion segmentation, video understanding, and gesture recognition. Optical flow, in particular, has been developed and improved in various ways for almost three decades. Several models and techniques have been proposed to enhance the quality of optical flow, since the first approach of Horn and Schunck [1] and Lucas-Kanade [2]. It is important to detect the object motion rather than pixel-wise intensity matching (e.g. optical flow) for real-life applications. Thus, the occlusion problem in optical flow estimation must be taken into account. The sharpness of the flow field along the object boundary is also important in the motion segmentation task.

The intensity difference constraint and the smoothness constraint, which are well-known in the literature, do not exactly describe the object movement in a real scene. In [3], the author tends to minimize the energy function with both the intensity constraint and smoothness constraint embedded inside. This model may hold in normal circumstances but not in the case of occlusion. In such a case, the intensity constraint does not hold. The flow field might be shifted to somewhere else but not the occluded area due to the energy function minimization. Thus, the partial differential equation (PDE)

* This research was supported by the MKE (The Ministry of Knowledge Economy), Korea, under the ITRC (Information Technology Research Center) support program supervised by the NIPA (National IT Industry Promotion Agency) (NIPA-2011-(C1090-1121-0008)), and by Priority Research Centers Program through the National Research Foundation of Korea (NRK) funded by the Ministry of Education, Science and Technology (2011-0018397).

Y.-S. Ho (Ed.): PSIVT 2011, Part I, LNCS 7087, pp. 73–84, 2011.

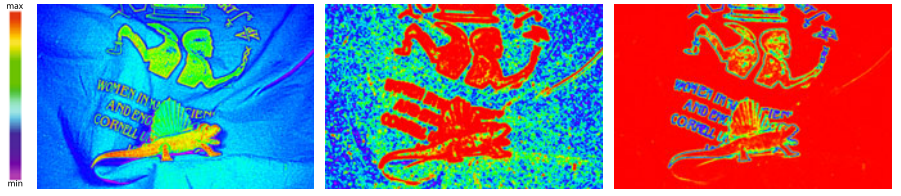

(a) (b) (c) (d)

Fig. 1. Visual result of adapting function on Dimetrodon sequence [10] (a) the color code for image and control functions, (b) enhanced image of frame 10, (c) data adapting-function f_d, (d) smoothness adapting-function

is no longer a favored tool to solve this problem as better solvers are available. In [4], the authors also use the variational model similar to [3] to initialize the flow field. They employ the color segmentation with flow field information to improve the estimation. Recently, [5] reveals excellent results performed by the variational model with the help of color information and improvements in the regularizers. Among the best, the total variational methods are also very strong solutions for this problem, as [6,7,8,9] yields the top results on Middlebury's website. So far, many improvements have been made to enhance the estimation result of optical flow. Yet, we can still push quality of optical flow estimation further. The key answer for this lies in the nature of object motion and the purpose of the estimation model. We will show how to improve a given model by using advanced scheme.

In this paper, we propose a model that can adapt the estimation process using the image information. We start from basic constraints of optical flow and use PDE solver for energy minimization to prove that our proposed method can improve the quality of the flow field. We propose the hybrid solver, which takes advantage of the multi-grid solver and coarse-to-fine estimation scheme, to deal with large displacement. With some small adaptations, we can even speed up the estimation process. Given an estimation model, our proposed scheme can push the quality of the estimation result further. The adapting functions and the hybrid scheme are the keys in our method. In the next section, we will discuss the proposed model and how the image information can be embedded in the model. We introduce details the hybrid scheme we use to solve the energy minimization problem in Section 3. We will detail the implementation and experiments in Section 4. We summarize the paper and outline on future work in Section 5.

2 Image-Adapting Energy Function

2.1 Optical Flow Constraints

Intensity Constraint. This constraint is the most basic constraint in every optical flow estimation model. It can be stated as follows

$$\mathbf{p} = \mathbf{argmin} |I_{t+\Delta t}(\mathbf{x}+\mathbf{p}) - I_t(\mathbf{x})| \tag{1}$$

where $I_t(\mathbf{x}) : \mathbb{R}^2 \mapsto \mathbb{R}$ denotes the image intensity of point (x,y) at time t with $\mathbf{x} = (x,y)^T$, and $\mathbf{p} = (u,v)^T$ is the motion vector between an image at time t and another

image at time $t+\Delta t$. This constraint is mostly described in the literature as the equation $I_{t+\Delta t}(\mathbf{x}+\mathbf{p}) - I_t(\mathbf{x}) = 0$; by which the linearized form yields the well-known optical flow constraint [1]:

$$I_x u + I_y v + I_t = 0. \tag{2}$$

The gradient constraint, conversely, is less sensitive to slight changes in brightness. However, it only holds when an object undergoes translation motion but not in the general case. Therefore, we only use the intensity constraint in the model.

Smoothness Constraint. This constraint states that the motion field must be smooth inside the object, even the object undergoes complex motion. In addition, the aperture problem occurs when the gradient disappears, or when the flow can only be detected in normal direction to the gradient. This is solved by considering the flow field smoothness. The flow field discontinues along the object boundary to achieve optimal estimation. With $f_s(\mathbf{x})$ as a function of image data, we formally express this piecewise smoothness constraint as follows

$$\mathbf{p} = \mathbf{argmin}\left(f_s(\mathbf{x})\left(|\nabla u|^2 + |\nabla v|^2\right)\right). \tag{3}$$

2.2 Adapting Functions

We arrive at the energy function used by previous work [3,11,12] using the above constraints:

$$\begin{aligned} E &= E_{data} + \beta E_{gradient} + \alpha E_{smooth} \\ &= \int_\Omega \left[\varphi_d(\mathbf{x},\mathbf{p}) + \beta\varphi_g(\mathbf{x},\mathbf{p}) + \alpha\varphi_s(\mathbf{x},\mathbf{p})\right] d\mathbf{x} \end{aligned} \tag{4}$$

where $\varphi_d(\mathbf{x},\mathbf{p})$, $\varphi_g(\mathbf{x},\mathbf{p})$ and $\varphi_s(\mathbf{x},\mathbf{p})$ are data term, gradient term and smoothness term respectively. In this work, we drop the gradient term, as mentioned above, and inject the adapting functions in the energy functions as follows:

$$\varphi_d(\mathbf{x},\mathbf{p}) = \varphi_d\left(f_d(\mathbf{x})|I_{t+\Delta t}(\mathbf{x}+\mathbf{p}) - I_t(\mathbf{x})|^2\right) \tag{5}$$

$$\varphi_s(\mathbf{x},\mathbf{p}) = \varphi_s\left(f_s(\mathbf{x})\left(|\nabla u|^2 + |\nabla v|^2\right)\right) \tag{6}$$

where f_d, f_s are adapting functions that will tune the estimation process using image information. The image itself contains much information. The idea is that we can suppress the difference of the data and flow, based on the features of the current pixel, given image information. In this way, the model can adapt to various kinds of image sequences and yields better estimation results.

Data Adaptation. We design f_d to suppress the difference in intensity of the points inside the object. First, the flow field inside the object must be smooth, since the smoothness constraint will drive the flow inside the object. Conversely, we can deal with the occlusion problem simultaneously. When a part of the object is occluded in the next frame, this data term still holds if the occluded area is inside the object. Fig. 1 shows the visual view of control functions on the Dimetrodon sequence [10].

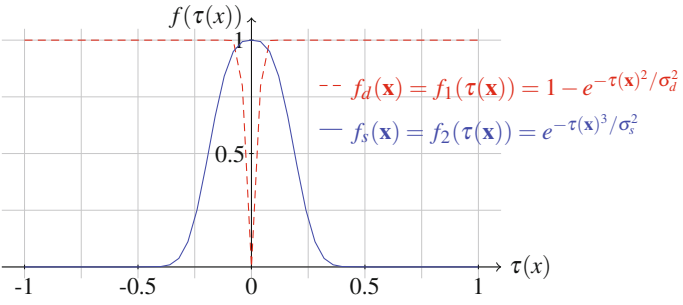

Fig. 2. Plot of control functions f_d(red dashed line) and f_s(blue line)

We can introduce several forms of f_d to yield the same effect based on the image features. Here, we introduce f_d as a function of gradient magnitude. Let $\tau(\mathbf{x}) = |\nabla I|$ be the magnitude of the image gradient at $\mathbf{x}$, then f_d can be simply defined as

$$f_d(\mathbf{x}) = f_1(\tau(\mathbf{x})) = 1 - e^{-\tau(\mathbf{x})^2/\sigma_d^2} \tag{7}$$

As in Fig. 2, the data difference is suppressed when the point is inside the homogenous area, e.g. $|\nabla I| \approx 0$. The data difference includes intensity difference, gradient difference, and other measurements, such as Hessian. In this work, we are concerned about the intensity difference in the model. Other measurements obviously can be controlled by this function, without a problem, since it is a function of spatial position. The parameter σ_d has an important role in the estimation result. We choose σ_d sufficiently small, so that it cannot create an over-smooth effect in the final result. Many experiments have been performed and we choose $\sigma_d = \sqrt{0.001}$ that yields the most stable results among test sequences.

Smoothness Adaptation. The function f_s should be large in homogenous area due to the smoothness energy (6), so that the flow field inside the object will be as smooth as possible. Similar to the data control function f_d above, f_s can be defined as follows

$$f_s(\mathbf{x}) = f_2(\tau(\mathbf{x})) = e^{-\tau(\mathbf{x})^\lambda/\sigma_s^2}. \tag{8}$$

where λ and σ_s are parameters controlling the shape of f_s. Setting λ to 2, we will get a similar form to f_d. However, this is not the case for f_s. The shape of function f_s must be wider and slowly drop, as in Fig. 2. When f_s drops too fast, the discontinuity of the flow will appear at some area where the gradient magnitude is larger than the specific threshold. This creates a segmentation effect on the flow field that we do not really want; especially, when the scene has smooth areas, where the gradient only changes a little bit from one to the next. This analysis leads to the f_s in (8) with $\lambda = 3$ and $\sigma_s = 0.1$. Other designs of f_d and f_s are available and can yield the same result, if they satisfy the above descriptions.

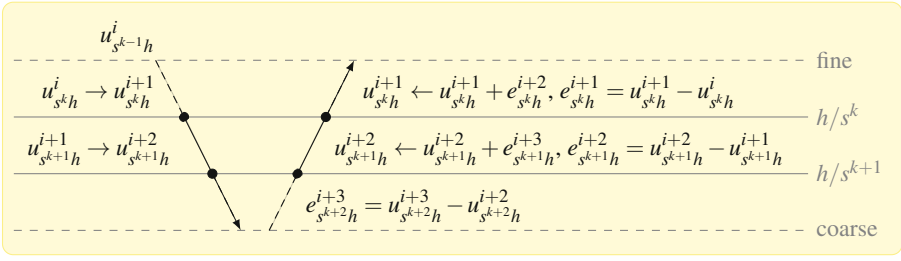

Fig. 3. Hybrid scheme is used to solve Euler-Lagrange equations with scale parameter s

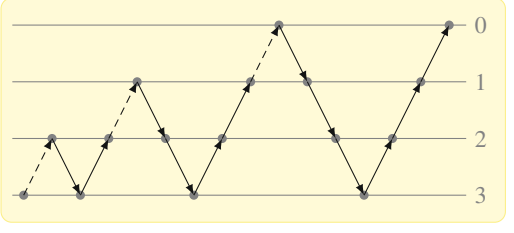

Fig. 4. Hybrid scheme with coarse-to-fine strategy

3 Hybrid Scheme for Energy Minimization

The energy function (4) now becomes

$$E = \int_\Omega \left[\varphi_d\left(\mathbf{x},\mathbf{p}\right) + \alpha\varphi_s\left(\mathbf{x},\mathbf{p}\right)\right] d\mathbf{x} \tag{9}$$

with the Euler-Lagrange equation system:

$$\begin{aligned} \varphi'_d\left(\bullet\right) f_d\left(\mathbf{x}\right) I_r I_x - \alpha \mathbf{div}\left(\varphi'_s(\bullet) f_s(\mathbf{x}) \nabla u\right) = 0 \\ \varphi'_d\left(\bullet\right) f_d\left(\mathbf{x}\right) I_r I_y - \alpha \mathbf{div}\left(\varphi'_s(\bullet) f_s(\mathbf{x}) \nabla v\right) = 0 \end{aligned} \tag{10}$$

where I_{*r} is the temporal difference

$$I_{*r} = I_{t+\Delta t,*}(\mathbf{x}+\mathbf{p}) - I_{t,*}(\mathbf{x}),$$

and I_* are the spatial derivatives in the next frame $I_{t+\Delta t,*}(\mathbf{x}+\mathbf{p})$. We choose the regularization functions φ_d, φ_s as $\varphi(s^2) = \sqrt{s^2+\varepsilon^2}$ that yields the total variation regularizer proposed in [13]. This regularizer leads to pseudo L_1-minimization. The quantity ε is chosen to be reasonably small, e.g. 0.001, to guarantee that φ is differentiable at $s = 0$.

The Euler-Lagrange equations are highly nonlinear due to the choice of φ_d and φ_s. The iteration scheme [12] is used to solve the flow field. It is necessary to approximate the global optimum of the energy using the iteration scheme and the multiscale

Algorithm 1. Mulrigrid scheme for flow estimation, V-cycle

if coarsest layer **then**
  Solve the flow field
else
  - Save result from previous step
  - Perform pre-relaxation on flow field
  - Restrict the flow to coarse layer
  Perform V-cycle on coarse layer
  - Calculate the error at coarse layer
  - Prolong the error to current layer
  - Update the flow at current layer
  - Perform post-relaxation on the flow
end if

approach. Let $\mathbf{p}^{(k)}$ be the flow field at step k, then the flow of the next iteration will be the solution of

$$\begin{aligned} 0 &= \varphi'_d(\bullet) f_d(\mathbf{x}) I_r^{(k+1)} I_x^{(k)} - \alpha \mathbf{div}\left(\varphi'_s(\bullet) f_s(\mathbf{x}) \nabla u^{(k+1)}\right) \\ 0 &= \varphi'_d(\bullet) f_d(\mathbf{x}) I_r^{(k+1)} I_y^{(k)} - \alpha \mathbf{div}\left(\varphi'_s(\bullet) f_s(\mathbf{x}) \nabla v^{(k+1)}\right) \end{aligned} \tag{11}$$

where

$$\begin{aligned} \varphi'_d(\bullet) &= \varphi'\left(f_d(\mathbf{x})\left(|I_{t+\Delta t}(\mathbf{x}+\mathbf{p})^{(k+1)} - I_t(\mathbf{x})|^2\right)\right), \\ \varphi'_s(\bullet) &= \varphi'\left(f_s(\mathbf{x})\left(|\nabla u^{(k+1)}|^2 + |\nabla v^{(k+1)}|^2\right)\right). \end{aligned}$$

The details of the discretization form can be derived easily, so we do not show them here. Both the coarse-to-fine scheme [3,5,12,14] and the multigrid scheme [11,15,16,17] have been used so far to solve (11) effectively. Here, we introduce the hybrid scheme to take advantage of the multigrid scheme and the coarse-to-fine scheme to produce an effective solver. The hybrid scheme is designed to solve (11) with an arbitrary scale parameter.

The purpose of the proposed scheme is to cope with large motion and improve the robustness of the solver simultaneously. While large motion can be detected at a coarse scale, the sharpness and precision of the flow field are enhanced at a fine scale. We build the pyramid of images and its derivative with the scale parameter s that can be larger than 0.5. The larger the value of s, the higher the computation cost. The idea of the multigrid solver is to solve the residual equations at the coarse layer and prolong the error from the coarse layer to the fine layer to correct the flow field. The flow is incrementally updated each iteration step as we use the iteration scheme. Thus, we employ the idea of the multigrid solver and form the scheme in Fig. 3.

Let $u^i_{s^k h}$ be the flow value at iteration ith on the kth layer in the pyramid model. Fig. 3 shows the basic V-cycle that we use to solve equation system. First, we perform the

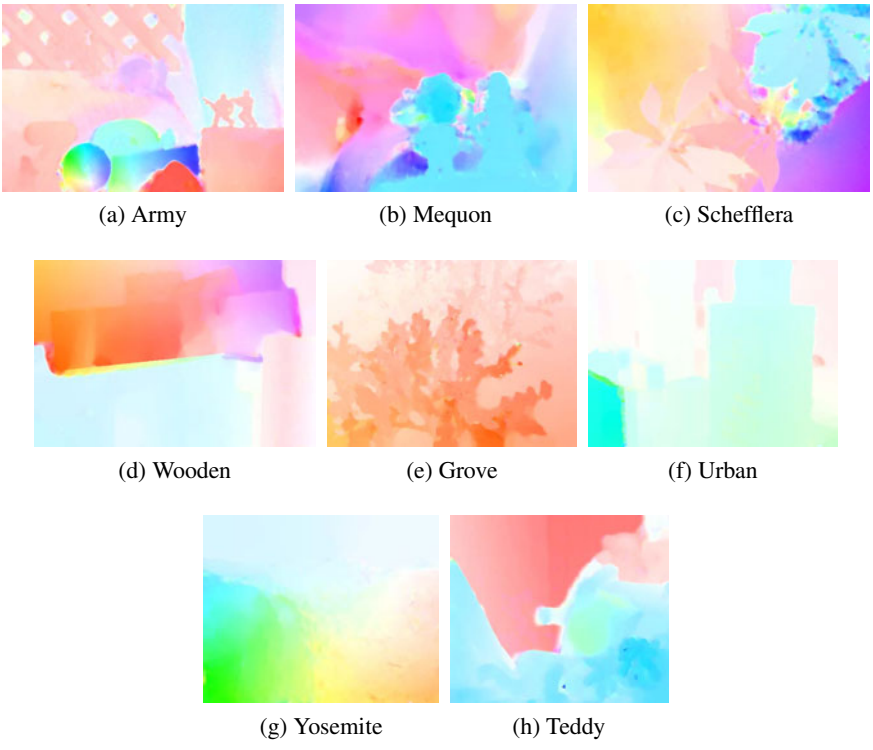

(a) Army (b) Mequon (c) Schefflera

(d) Wooden (e) Grove (f) Urban

(g) Yosemite (h) Teddy

Fig. 5. Visual result of our method on evaluation sequences from Middlebury's dataset [10]

relaxation step on flow $u^i_{s^k h}$ to yield $u^{i+1}_{s^k h}$. The flow $u^{i+1}_{s^k h}$ is restricted to a coarser layer, as $u^{i+1}_{s^{k+1} h}$ with the scale factor s. This pre-relaxation step and restriction step continue until we reach the coarsest layer. At this stage, we can simply calculate the error, as the difference between the final result and the restricted result from the fine layer. As we have the error at a certain layer, say $e^{i+2}_{s^{k+1} h}$, we can propagate it to a finer layer, as $e^{i+2}_{s^k h}$ with the scale factor s^{-1}. The flow is updated using this error as follows

$$u^{i+1}_{s^k h} \leftarrow u^{i+1}_{s^k h} + e^{i+2}_{s^k h}$$

We perform post-relaxation on the flow $u^{i+1}_{s^k h}$ once again, before calculating the error at the current layer and propagating it to the finer layer. This process repeats until we reach the finest layer. Fig. 3 and algorithm 1 summarize the details of this scheme.

The coarse-to-fine strategy is used along with the V-cycle that we described above to deal with large motion. We perform the V-cycle on each layer. The result is then propagated to the finer layer with scale factor s^{-1}. This process is repeated from the coarsest layer to the finest layer, as in Fig. 4. We can achieve a good result with only a few iterations at each relaxation step. In the experiment, we use five iterations for each relaxation step.

4 Experiments

The quality of flow field is evaluated by angular error and end-point error. Some other measurements are also used but they are not comparable in the context of object movement. The angular error is given as follows:

$$e_\theta = \arccos\left(\frac{\mathbf{p}^T\mathbf{p}_{gt}+1}{\sqrt{\mathbf{p}^T\mathbf{p}+1}\sqrt{\mathbf{p}_{pt}^T\mathbf{p}_{pt}+1}}\right) \tag{12}$$

where $\Delta t = 1$ and $\mathbf{p}_{gt} = (u_{gt}, v_{gt})$ is the true motion field of the current image.

Table 1. Estimation results on synthetic training sequences [10]

Sequence	AEE	STD	AAE	STD
Dimetrodon	0.154	0.154	2.667	2.598
Grove2	0.246	0.435	3.509	6.972
Grove3	0.687	1.424	6.910	16.613
Hydrangea	0.181	0.376	2.221	5.574
RubberWhale	0.128	0.324	4.247	11.799
Urban2	0.427	1.276	3.199	8.319
Venus	0.332	0.604	4.718	13.356

4.1 Synthetic Images

First, the experiments were performed on the training data with available groundtruths. Our proposed flow field is very sharp along the object boundary. Table 1 gives the quantitative evaluation, where AEE is the average end-point error, AAE is the average angular error, and STD is the standard deviation of those two errors. We perform experiments on these training sequences to get the parameter set that yield the most stable results through difference sequences. Even though the smooth parameter can be embedded inside the control function, we still keep it as additional parameter for our experiments.

The proposed model does not operate at its best, as we are using the grayscale image, since much information has been discarded. In addition, it is hard to specify which point belongs to object by its color, because the color range is limited on the grayscale image. Therefore, comparing our method to other methods operating on color images is unfair. However, even if the grayscale image limits our model, we still obtained some good results, as shown in Table 1.

We also performed the experiments with the evaluation dataset on Middlebury's website [10] to show how the proposed model can improve a given model. We start from a very basic model, which is close to the model in [14]. We even discard the gradient term in the model. We choose this basic model, as it can easily reveal the performance

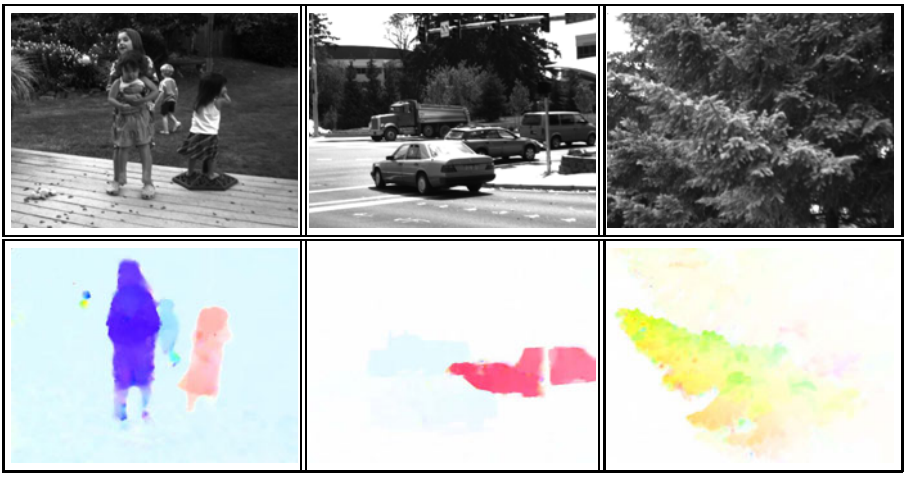

(a) (b) (c)

Fig. 6. Estimation result of our method on some evaluation sequences from MiddleBury's dataset [10]. First row is frame 10 and second row is the estimated flow field. (a) Backyard, (b) Dumptruck, (c) Evergreen.

of our proposed model and our optimization scheme. It is very hard to see how good the result is for advanced models in the top of Middlebury's list. The results at the top of the table are very close to one another.

Second column of Table 2 shows the results with the present of Hybrid scheme. The results in first column are obtained with the used of control functions and the multiscale approach. As we see here, the Hybrid scheme reduces the end-point error for most of evaluation sequences comparing to the traditional multiscale approach. The Hybrid scheme gives about the same performance as multiscale approach for Urban, Yosemite, and Teddy. However, it still improves the end-point error 9% accuracy in average (30% on Mequon sequence, 33% on Wooden sequence, 23% on Army). A similar observation can be seen in Table 3. It reduces 5% of angular error in average (31% on Mequon and Wooden sequence). As a result, the Hybrid scheme shows that it can cope with large motion as multiscale approach and slightly improves accuracy of the flow field. These results consistently show the improvement of our proposed method compared to the original model. Our method yields better results than some of the current state-of-art methods [4,5,18,19,20,21,22,23,24] for Urban sequence. A similar observation can be seen on the Grove sequence. The angular errors on Urban, Teddy, and Yosemite sequences are higher when we apply the Hybrid scheme. The reason for large error on these sequences comes from low contrast image (Urban, Yosemite) and low texture (top right side of Teddy). Thus, additional correction step can be applied to push the accuracy further.

Table 2. End-point error on evaluation sequences [10]

Sequence	with adapting functions	+ hybrid scheme
Army	0.22	0.17
Mequon	0.87	0.61
Schefflera	1.17	1.20
Wooden	0.99	0.66
Grove	1.17	0.99
Urban	0.72	0.73
Yosemite	0.14	0.18
Teddy	1.37	1.30

Table 3. Angular error on evaluation sequences [10]

Sequence	with adapting functions	+ hybrid scheme
Army	7.88	6.49
Mequon	13.4	9.22
Schefflera	17.6	16.4
Wooden	12.0	8.22
Grove	4.38	3.77
Urban	5.69	6.84
Yosemite	2.75	3.59
Teddy	6.59	7.51

4.2 Real-Life Images

We are interested in the results on real-life sequences for applications. Therefore, we performed the method on some real-life sequences to prove how effective it is for real applications. Middlebury's website has another measurement, termed interpolation error, beside the end-point error and angular error. This measurement, however, does not completely hold in our case. As we are interested in the object movement, rather than intensity matching, the interpolation error can be large due to the occlusion problem. Thus, the evaluation results on interpolation error cannot be compared in our case.

Fig. 6 shows some results on real-life sequences of the evaluation dataset [10]. The discontinuity of the flow field along the object boundary is highly preserved. Other experiments are performed on real-life sequences from the training dataset [10]. Fig. 7 shows some visual results on these sequences. The results on the DogDance sequence and MiniCooper sequence are proof for the effectiveness of our proposed method. The proposed method indeed improves the smoothness of flow field, while retaining the sharpness on edge in case of DogDance and MiniCooper sequences. This is especially helpful when we use the result for motion segmentation, object isolation, etc. We can see that our method outperforms the original model. We achieve the sharpness, the smoothness, and solve the occlusion problem simultaneously. Our proposed method shows how we can improve performance of a given estimation model further.

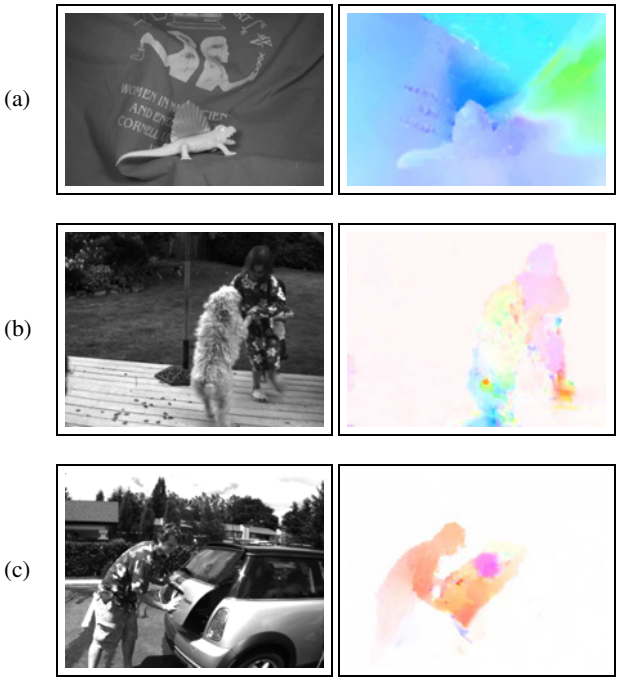

Fig. 7. Estimation result of our method on other real-life sequences [10]. (a) Dimetrodon, (b) DogDance, (c) MiniCooper.

5 Conclusion

We proposed an improved algorithm for optical flow estimation using the variational model. The image information was used to tune the estimation process. We introduced the adapting functions and embedded them to the energy function. Our model also addressed the occlusion problem. We proposed a hybrid scheme that took advantage of the coarse-to-fine approach and the multigrid solver to yield more robust results. The result with the present of hybrid solver and control functions was indeed much better and more robust.

We are applying the method for grayscale images. Further work includes the extension of our approach to color images. Our approach can also be integrated into advanced models to produce even better results. An in-depth study of the effect of our method on advanced models may lead to some interesting results in the near future.

References

1. Horn, B.K.P., Schunck, B.G.: Determining optical flow. Artificial Intelligence 17(1-3), 185–203 (1981)
2. Lucas, B.D., Kanade, T.: An iterative image registration technique with an application to stereo vision. In: IJCAI, pp. 674–679 (April 1981)

3. Brox, T., Bruhn, A., Papenberg, N., Weickert, J.: High Accuracy Optical Flow Estimation Based on a Theory for Warping. In: Pajdla, T., Matas, J(G.) (eds.) ECCV 2004. LNCS, vol. 3024, pp. 25–36. Springer, Heidelberg (2004)
4. Xu, L., Chen, J., Jia, J.: A Segmentation Based Variational Model for Accurate Optical Flow Estimation. In: Forsyth, D., Torr, P., Zisserman, A. (eds.) ECCV 2008, Part I. LNCS, vol. 5302, pp. 671–684. Springer, Heidelberg (2008)
5. Zimmer, H., Bruhn, A., Weickert, J., Valgaerts, L., Salgado, A., Rosenhahn, B., Seidel, H.-P.: Complementary Optic Flow. In: Cremers, D., Boykov, Y., Blake, A., Schmidt, F.R. (eds.) EMMCVPR 2009. LNCS, vol. 5681, pp. 207–220. Springer, Heidelberg (2009)
6. Wedel, A., Pock, T., Braun, J., Franke, U., Cremers, D.: Duality tv-l1 flow with fundamental matrix prior. In: Image and Vision Computing New Zealand (2008)
7. Werlberger, M., Pock, T., Bischof, H.: Motion estimation with non-local total variation regularization. In: CVPR, pp. 2464–2471 (2010)
8. Wedel, A., Pock, T., Zach, C., Bischof, H., Cremers, D.: An Improved Algorithm for TV-L1 Optical Flow. In: Cremers, D., Rosenhahn, B., Yuille, A.L., Schmidt, F.R. (eds.) Statistical and Geometrical Approaches to Visual Motion Analysis. LNCS, vol. 5604, pp. 23–45. Springer, Heidelberg (2009)
9. Werlberger, M., Trobin, W., Pock, T., Wedel, A., Cremers, D., Bischof, H.: Anisotropic huber-l1 optical flow. In: BMVC, British Machine Vision Association (2009)
10. Baker, S., Scharstein, D., Lewis, J.P., Roth, S., Black, M.J., Szeliski, R.: A database and evaluation methodology for optical flow. In: ICCV, pp. 1–8 (2007)
11. Bruhn, A., Weickert, J.: Towards ultimate motion estimation: combining highest accuracy with real-time performance. In: ICCV, vol. 1, pp. 749–755 (October 2005)
12. Papenberg, N., Bruhn, A., Brox, T., Didas, S., Weickert, J.: Highly accurate optic flow computation with theoretically justified warping. Int. J. Comput. Vision 67(2), 141–158 (2006)
13. Rudin, L.I., Osher, S., Fatemi, E.: Nonlinear total variation based noise removal algorithms. Phys. D 60(1-4), 259–268 (1992)
14. Bruhn, A., Weickert, J., Schnörr, C.: Lucas/kanade meets horn/schunck: Combining local and global optic flow methods. Int. J. Comput. Vision 61(3), 211–231 (2005)
15. Bruhn, A., Weickert, J., Feddern, C., Kohlberger, T., Schnörr, C.: Variational optic flow computation in real-time. IEEE Trans. Image Proc. 14(5), 608–615 (2005)
16. Bruhn, A., Weickert, J., Kohlberger, T., Schnörr, C.: Discontinuity-Preserving Computation of Variational Optic Flow in Real-Time. In: Kimmel, R., Sochen, N.A., Weickert, J. (eds.) Scale-Space 2005. LNCS, vol. 3459, pp. 279–290. Springer, Heidelberg (2005)
17. Bruhn, A., Weickert, J., Kohlberger, T., Schnörr, C.: A multigrid platform for real-time motion computation with discontinuity-preserving variational methods. Int. J. Comput. Vision 70(3), 257–277 (2006)
18. Lei, C., Yang, Y.-H.: Optical flow estimation on coarse-to-fine region-trees using discrete optimization. In: ICCV, pp. 1562–1569 (2009)
19. Lee, K.J., Kwon, D., Yun, I.D., Lee, S.U.: Optical flow estimation with adaptive convolution kernel prior on discrete framework. In: CVPR, pp. 2504–2511. IEEE (2010)
20. Lempitsky, V.S., Roth, S., Rother, C.: Fusionflow: Discrete-continuous optimization for optical flow estimation. In: CVPR (2008)
21. Glocker, B., Paragios, N., Komodakis, N., Tziritas, G., Navab, N.: Optical flow estimation with uncertainties through dynamic mrfs. In: CVPR (2008)
22. Seitz, S.M., Baker, S.: Filter flow. In: ICCV, pp. 143–150 (2009)
23. Sun, D., Roth, S., Lewis, J.P., Black, M.J.: Learning Optical Flow. In: Forsyth, D., Torr, P., Zisserman, A. (eds.) ECCV 2008, Part III. LNCS, vol. 5304, pp. 83–97. Springer, Heidelberg (2008)
24. Li, Y., Huttenlocher, D.P.: Learning for Optical Flow Using Stochastic Optimization. In: Forsyth, D., Torr, P., Zisserman, A. (eds.) ECCV 2008, Part II. LNCS, vol. 5303, pp. 379–391. Springer, Heidelberg (2008)